Chapter 4 Phonon Calculation and Layer/ Morphology/ Substrate Dependence on Anisotropic Response of MoS_2

4.1 Introduction

Nowadays, polarization resolved imaging based on polarization of electric field, is receiving intense attraction for application in finger printing, recognition of astronomical objects, military surveillance, etc. and in biomedical applications like retinal surgery imaging, cancer detection at early stages, etc. [129-134]. For these applications, it is required to control the polarization and direction of scattered light. Angle resolved polarized Raman spectroscopy (ARPRS) is a useful tool that reveals the anisotropic behavior of materials by probing the interaction mechanism of electrons with phonons and photons in light matter interaction and plays a key role for essential designing of improved optoelectronic devices. The ARPRS study can be inspected by examining the periodical change in the intensity of Raman modes by varying the polarization of incident light during the measurement and also allows to identify the symmetries of the detected phonon modes [135]. Therefore, it's natural that the ARPRS can also be employed for the determination of crystalline orientation and mode's symmetry [136]. The optical anisotropic response of these materials promises the wide-open field prospective applications in MoS_2-based photonic and optoelectronic devices like polarization-sensitive photodetectors, phototransistors, linearly polarized pulses generators, optical waveplates, optical switches and interconnects, etc. [137-141]. The real device configuration demands the large area and high-quality films with controllable layer number showing excellent properties, which can be obtained via CVD method. In literature mostly the anisotropic behavior of MoS_2 has been reported on mechanically exfoliated samples, which have limitation over scalability for device application. In this chapter, we examine theoretically the possible phonon modes in different layered MoS_2 nanostructures using group theory and density functional perturbation

theory (DFPT). The phonon dispersion curve along with their phonon density of states (DOS) for 1 to 6L (L is the layer number) MoS_2 shows the evolution of phonon modes with increasing layer number and contribution of each atom to the total phonon DOS, respectively. Further, we report the systematic optical anisotropy study of layer dependent (1L, 3L and 5L) CVD grown triangular MoS_2 nanostructure using ARPRS study under non-resonant (532 nm) and resonant (633 nm) excitation wavelengths to observe the electron-phonon-photon coupling effect. Intensity profile of each phonon mode has been analyzed as a function of polarization angle. An unexpected behavior in polarised Raman study of E^1_{2g} phonon mode is observed with 633 nm excitation, in contrast to 532 nm excitation wavelength, owing to Frohlich exciton-phonon interaction. This behavior has been discussed based on electron-phonon-photon interaction to explain the polarization behavior of phonon modes as a function of layer number and incident excitation wavelength. Next, to illustrate the effect of orientation of nanostructure film on anisotropic response, the ARPRS study of horizontally and vertically oriented MoS_2 (H-MoS_2/SiO_2-Si and V-MoS_2/SiO_2-Si) nanostructures has been performed. We also performed similar study on large area thin film of horizontally oriented MoS_2 grown over conducting substrate, i.e. on H-MoS_2/FTO.

4.2 Results and Discussion

4.2.1 Group Theory and Phonon Dispersion for Different Layered (1 to 6L) MoS_2

Firstly, we use the group theory to analyse the symmetry-related information. Bulk 2H-MoS_2 belongs to the D_{6h} point group and the irreducible representations of the phonon modes at Γ-point is given by $\Gamma_{bulk} = A_{1g} + 2A_{2u} + 2B_{2g} + B_{1u} + E_{1g} + 2E_{1u} + E_{2u} + 2E_{2g}$ [142, 143]. On reducing the number of layers (N) from bulk to few layers, the symmetry operations are also reduced. **Figure 4.1 (a, d)** shows the top view and **Figure 4.1 (b, e)** shows the side view of 1L (odd) and 2L (even) MoS_2, respectively. The odd L has D_{3h} point group and the symmetry operations present are: E (identity), $2C_3$ (three fold clockwise and anticlockwise rotation about

the z-axis, as shown in **Figure 4.1 (b)**), $3C_2'$ (three two fold rotation about the axis marked by the red dash line in **Figure 4.1 (c)**), σ_h (horizontal plane of symmetry that is perpendicular to the C_3 axis and passes through the Mo atom), $3\sigma_v$ (vertical plane of symmetry that is parallel to the C_3 axis) and $2S_3$ (C_3 rotation followed by reflection via σ_h). The even L has D_{3d} point group and symmetry elements present are: E, $2C_3$, $3C_2'$, i (inversion), $3\sigma_d$ (dihedral plane of symmetry, as shown in **Figure 4.1 (f)**) and $2S_6$ (C_6 rotation followed by reflection via σ_h) [144, 145]. Lattice vibrations irreducible representations is given by the relation $\Gamma^{vib} = (\Gamma^{eq} \otimes \Gamma^{vec}) - \Gamma^{trans} - \Gamma^{rot}$, where Γ^{eq} is the equivalent representation for atomic sites and Γ^{vec} is the representations for x, y, z vector, Γ^{trans} and Γ^{rot} represents the translations and rotations of the molecule respectively [145, 146]. So, to acquire the 9L normal vibration modes in L-MoS_2 (L is the layer number), Γ^{vib} is expressed in irreducible representation of point group.

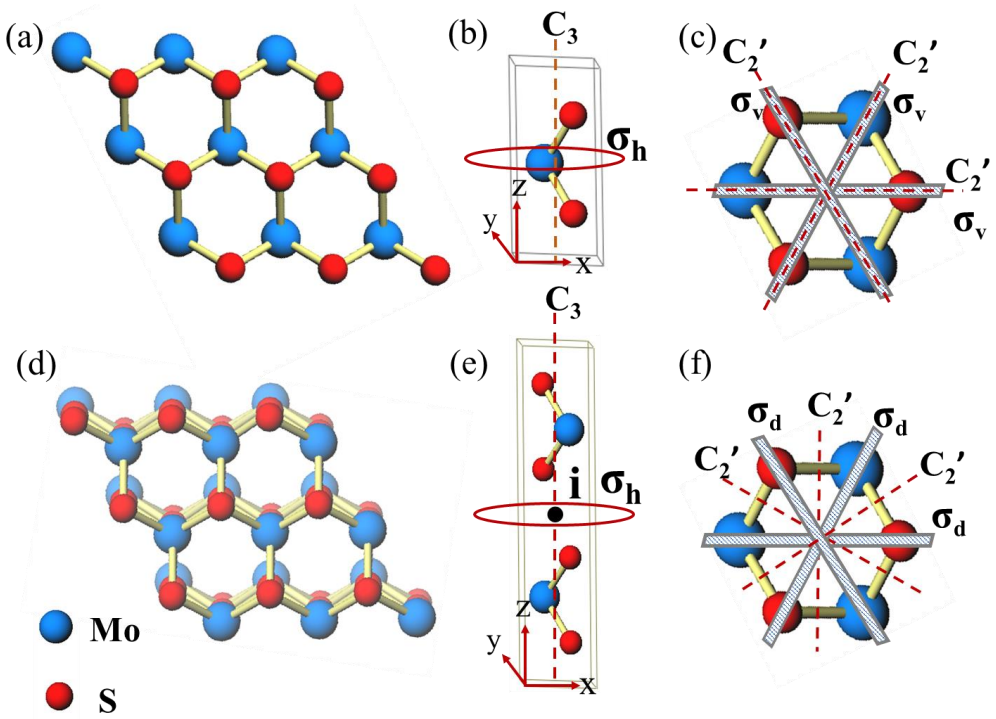

Figure 4.1 *Symmetry operations in 1L (odd L) and 2L (even L) 2H-MoS_2. (a, d) shows the top view for 1L and 2L, respectively. (b, e) shows the side view of respective layers with C_3 symmetry operation along the marked axis and red color circle represents the σ_h reflection plane. The black dot at the centre in (e) illustrates the inversion symmetry. (c, f) shows three C_2' symmetry along the red dotted line in the xy plane, σ_v and σ_d operation is shown by the mirror plane.*

In general, the normal vibrational modes for odd and even number of layers at zone centre is given by the following irreducible representation using character table (**Table 4.1** and **Table 4.2**) [146, 147]-

$$\Gamma_{odd} = \left(\frac{3L-1}{2}\right)(A_1' + E'') + \left(\frac{3L+1}{2}\right)(A_2'' + E') \text{ and } \Gamma_{even} = \left(\frac{3L}{2}\right)(A_{1g} + A_{2u} + E_g + E_u)$$

Thus, 1L MoS_2 constitutes 9 vibration modes at Γ point and is given by Γ (1L) = $2A_2'' + A_1' + 2E' + E$.

Table 4.1 Character table for D_{3h} point group

Quadratic	**Linear, rotations**	**SG**	**PG**	**E**	**$2C_3$**	**$3C_2'$**	**σ_h**	**$2S_3$**	**$3\sigma_v$**
x^2+y^2, z^2		Γ_1^+	A_1'	1	1	1	1	1	1
	R_z	Γ_2^+	A_2'	1	1	-1	1	1	-1
(x^2-y^2, xy)	(x, y)	Γ_3^+	E'	2	-1	0	2	-1	0
		Γ_1^-	A_1''	1	1	1	-1	-1	-1
	z	Γ_2^-	A_2''	1	1	-1	-1	-1	1
(xz, yz)	(R_x, R_y)	Γ_3^-	E''	2	-1	0	-2	1	0

Table 4.2 Character table for D_{3d} point group

Quadratic	**Linear, rotations**	**SG**	**PG**	**E**	**$2C_3$**	**$3C_2'$**	**i**	**$2S_6$**	**$3\sigma_d$**
x^2+y^2, z^2		Γ_1^+	A_{1g}	1	1	1	1	1	1
	R_z	Γ_2^+	A_{2g}	1	1	-1	1	1	-1
$(xz,yz),(x^2-y^2,xy)$	(R_x, R_y)	Γ_3^+	E_g	2	-1	0	2	-1	0
		Γ_1^-	A_{1u}	1	1	1	-1	-1	-1
	z	Γ_2^-	A_{2u}	1	1	-1	-1	-1	1
	(x, y)	Γ_3^-	E_u	2	-1	0	-2	1	0

The schematic vibrations of the phonon modes for 1L MoS_2 are shown in **Figure 4.2 (a)**. The phonon mode A_1' and E " are induced by the vibration of S atoms, while A''_2 and E ' modes have contributions from the vibrations of both the Mo and S atoms. One A_2'' and one E′ mode

comprises the acoustic modes, while rest are the optical modes. Similarly, 2L MoS_2 is characterized by 18 vibration modes at Γ point and is given by $\Gamma(2L) = 3A_{1g} + 3A_{2u} + 3E_g + 3E_u$, where one A_{2u} and E_u comprises the acoustic modes. The schematic vibrations of the phonon modes for 2L MoS_2 are shown in **Figure 4.2 (b)**. On moving from 1L to 2L, the 9 phonon modes are split into 18 phonon modes (3 acoustic and 15 optical modes), as shown in **Figure 4.2 (c)**.

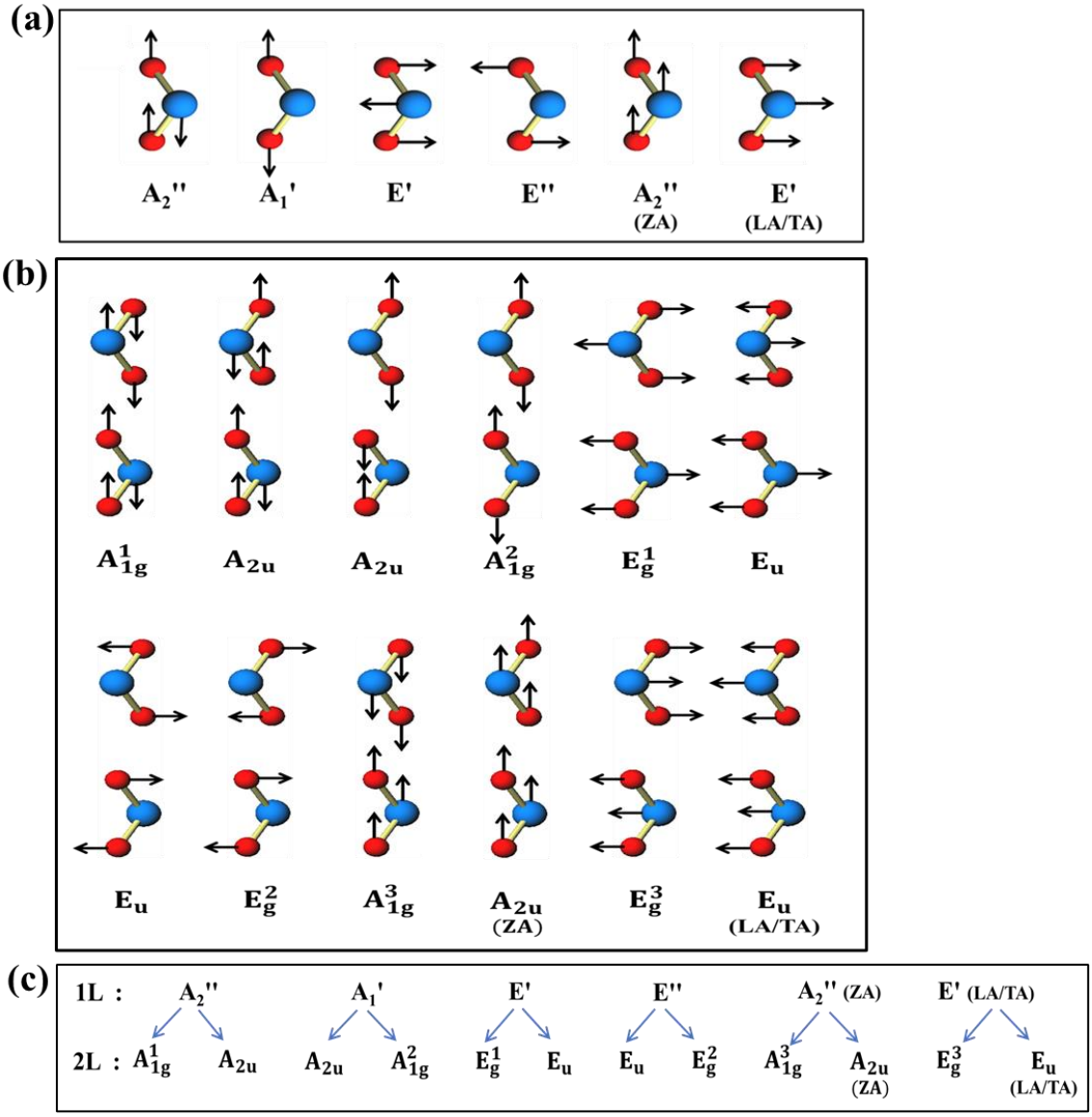

Figure 4.2 *Schematic showing the phonon vibrations in (a) 1L and (b) 2L MoS_2. (c) Each phonon mode in 1L MoS_2 are split into two phonon modes in 2L MoS_2.*

The phonon dispersion and their corresponding partial phonon DOS calculations have been performed for different layered MoS_2 by density functional perturbation theory (DFPT)

using Quantum Espresso module [114]. The local density approximation (LDA) with Perdew-Zunger for electron exchange-correlation functional and Trouiller-Martins type norm-conserving pseudopotentials were used [148, 149]. Firstly, a 2D slab was modelled for different layered MoS_2 by applying periodic boundary conditions in x- and y- direction and adding a vacuum layer of 15 Å along z direction to ensure that there is no suspicious interaction between layers. Then, the structure was relaxed by applying force convergence threshold of 10^{-6} a.u. and the kinetic energy cut-off for wavefunction was set at 70 Rydberg (Ry). Then the phonon frequencies of different layered (1 to 6L) MoS_2 were computed from the relaxed hexagonal crystal structure at gamma centred 4×4×1 q-mesh of the first Brillouin Zone (BZ), along high symmetry directions Γ−M−K−Γ. **Figure 4.3 (a-f)** shows the calculated phonon dispersion curve along with phonon DOS of 1 to 6L MoS_2. The positive phonon frequencies in the first BZ clearly shows the dynamical stability of different layered MoS_2 nanostructures. The phonon dispersion curve of 1L MoS_2 (**Figure 4.3 (a)**) shows nine vibrational modes, of which three are acoustic and six are optical phonon modes. The acoustic branch comprises of longitudinal acoustic (LA), transverse acoustic (TA) and flexural (out of plane) acoustic (ZA) branches. Around Γ point, the LA and TA branches (E') are linear and the ZA branch (A_2") is quadratic, owing to low lattice dimensionality and at Γ point, the frequencies of all these three acoustic modes becomes zero. The six optical branches correspond to the irreducible representations E" (LO_1 and TO_1), E' (LO_2 and TO_2), A_2" (ZO_1) and A_1' (ZO_2). Here, (LO_1 and LO_2) represents the two in-plane longitudinal, (TO_1 and TO_2) represents the two in-plane transverse and (ZO_1 and ZO_2) represents the two out of plane optical branches. A small LO-TO splitting (~2 cm^{-1}) at Γ point is observed, owing to lattice vibration coupling with the polarization effect and thus can be neglected [150]. **Table 4.3** shows good correspondence between calculated and experimental frequencies of the four optical phonon modes at Γ point of MoS_2. The calculated evident gap between the acoustic and optical branches is ~49 cm^{-1}, which is in good agreement

with previous theoretical results [151, 152]. The phonon DOS shows each atom's contribution to the total phonon DOS and is consistent with the dispersion curve. The phonon DOS for 1L MoS_2 displays that the intermediate optical modes have contributions from vibrations of S atom while the acoustic and higher optical modes have contributions from vibrations of both Mo and S atom. Owing to weak van der Waals interaction in layered MoS_2, the frequency splitting between two optical branches, stemming from a single optical branch, is very small and thus the phonon dispersion curves for different layer number resembles each other. In different layered MoS_2, we observe that each acoustic mode consists of N branches (LA_i, TA_i and ZA_i, where i = 1,2,...N) and these N branches overlap or becomes degenerate on going away from first BZ.

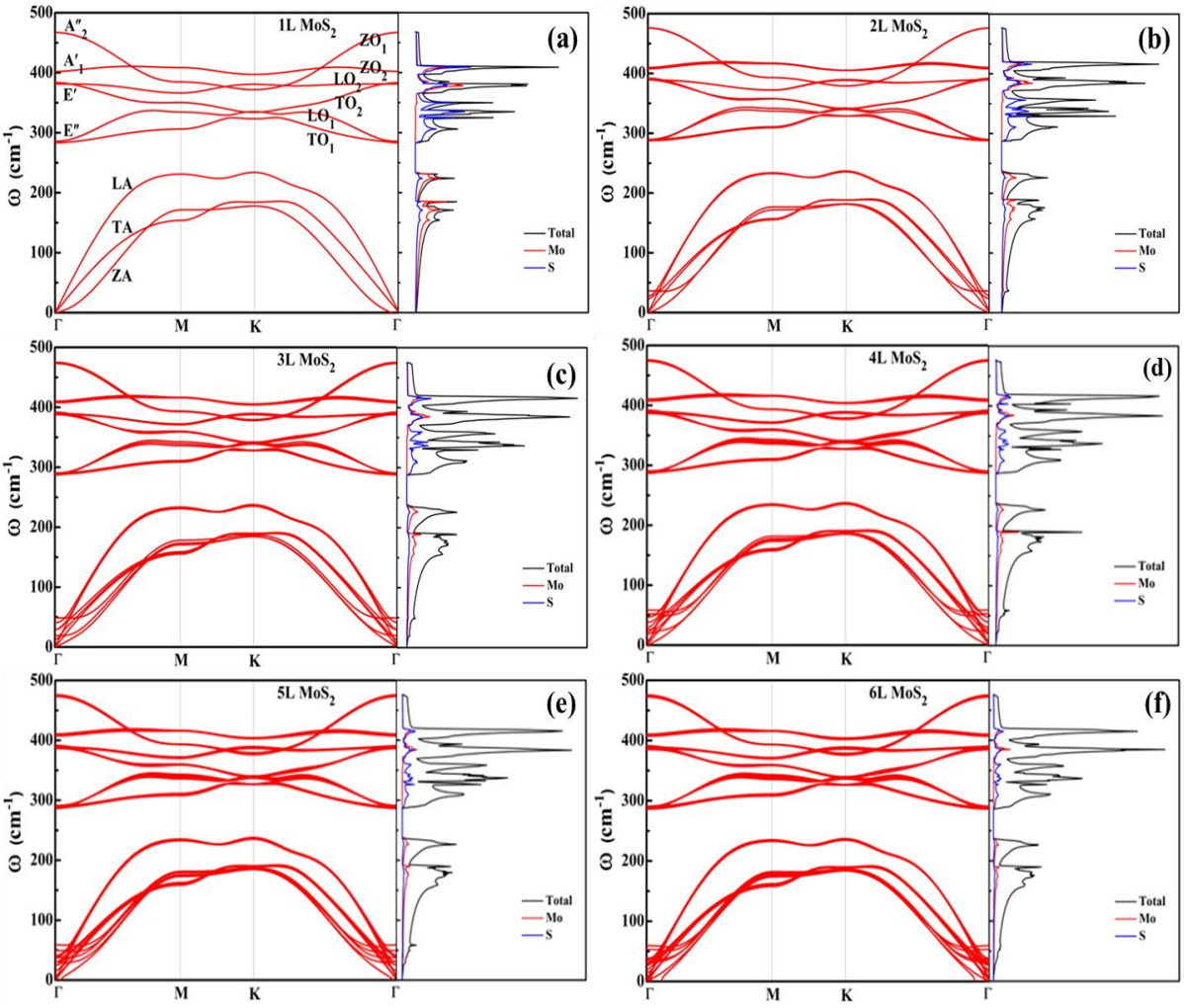

Figure 4.3 *(a-f) Phonon dispersion curve along with phonon DOS for 1 to 6L MoS_2.*

Table 4.3 Comparison of theoretically obtained frequencies of optical phonon modes at Γ point in 1L MoS_2 with experimentally reported data (in units of cm^{-1}).

	E ''	**E '**	**A_1'**	**A_2''**
Calculated (Present work)	283.3	381.3	402.1	467.0
Experimental [153]	287	383.5	402.4	470

4.2.2 ARPRS Study

After theoretical observation of phonon modes, we have performed ARPRS study of different prepared MoS_2 samples to examine the anisotropic behavior of phonon modes. Usually ARPRS study can be demonstrated in three typical polarization arrangements: 1) The incident laser polarization ($\hat{g}_i$) is kept fixed and the polarization of the scattered laser light ($\hat{g}_s$) is changed using an analyzer or vice-versa setup i.e. $\hat{g}_i$ is varied with fixed analyzer; 2) By changing the $\hat{g}_i$ and $\hat{g}_s$ simultaneously; 3) By fixing the $\hat{g}_i$ and $\hat{g}_s$ with sample rotation around the laser. Here, we have followed the second arrangement, i.e., the incident polarization direction was varied using half waveplate ($\alpha/2$ = 0º, 45º, 90º and 135º) and the polarization direction of the scattered beam was varied using analyzer at an interval of 10° from θ = 0º to 90º, thus covering the complete rotation from 0º to 360º. Thus, the scattered light lies within the XY plane. All the measurements were carried out in backscattering geometry with 532 and 633 nm excitation source and the Raman spectra were collected by STR-300 spectrometer using 1200 cm^{-1} grating with 100x objective lens. **Figure 4.4** shows the schematic of the typical experimental setup for ARPRS study with sketched $\hat{g}_i$, $\hat{g}_s$ and θ.

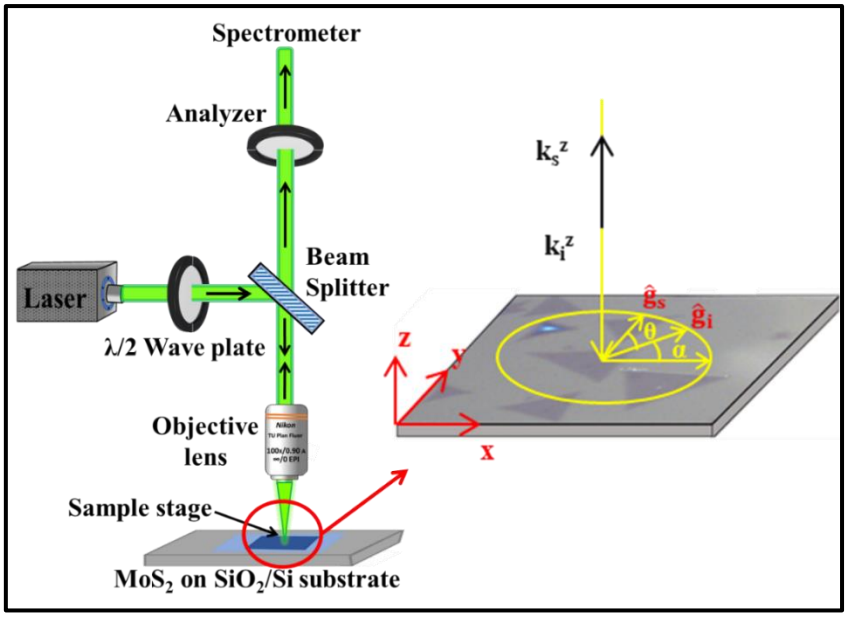

Figure 4.4 *Schematic diagram depicting the experimental setup with backscattering geometry for demonstrating the ARPRS study of CVD grown triangular MoS_2.*

4.2.3 ARPRS Study of CVD Grown 1L, 3L and 5L Triangular MoS_2/SiO_2-Si

In this section, we investigate the optical anisotropic response of Raman modes using ARPRS study for CVD-grown triangular MoS_2 nanostructures with different layer numbers (1L, 3L and 5L) under non-resonant (532 nm) and resonant (633 nm) excitations. We discuss the theory for explaining the polarization response as a function of layer number and excitation wavelength.

4.2.3.1 Characterization of CVD Grown Triangular MoS_2/SiO_2-Si

Figure 4.5 (a) shows the optical image of different layered MoS_2 domains with triangular structure of different sizes. **Figure 4.5 (b-d)** shows the confocal mapping of Raman spectra for 1L, 3L and 5L triangular MoS_2 on the same color scale, respectively, with the corresponding optical image shown in inset. The edges of vertically stacked triangular MoS_2 nanoflakes are observed to be in parallel with the basal plane of triangular monolayer MoS_2, showing no stacking misalignment with neighbouring layers. The Raman intensity map of 1L shows the homogeneous intensity distribution (**Figure 4.5 (b)**), indicating the smoothness and uniformity of the grown monolayer island. Whereas for the 3L (**Figure 4.5 (c)**) and 5L (**Figure**

4.5 (d)), the centre part of the triangular MoS_2 island is brighter compared to the outer region, indicating the growth via layer-by-layer stacking of MoS_2 in vertical direction.

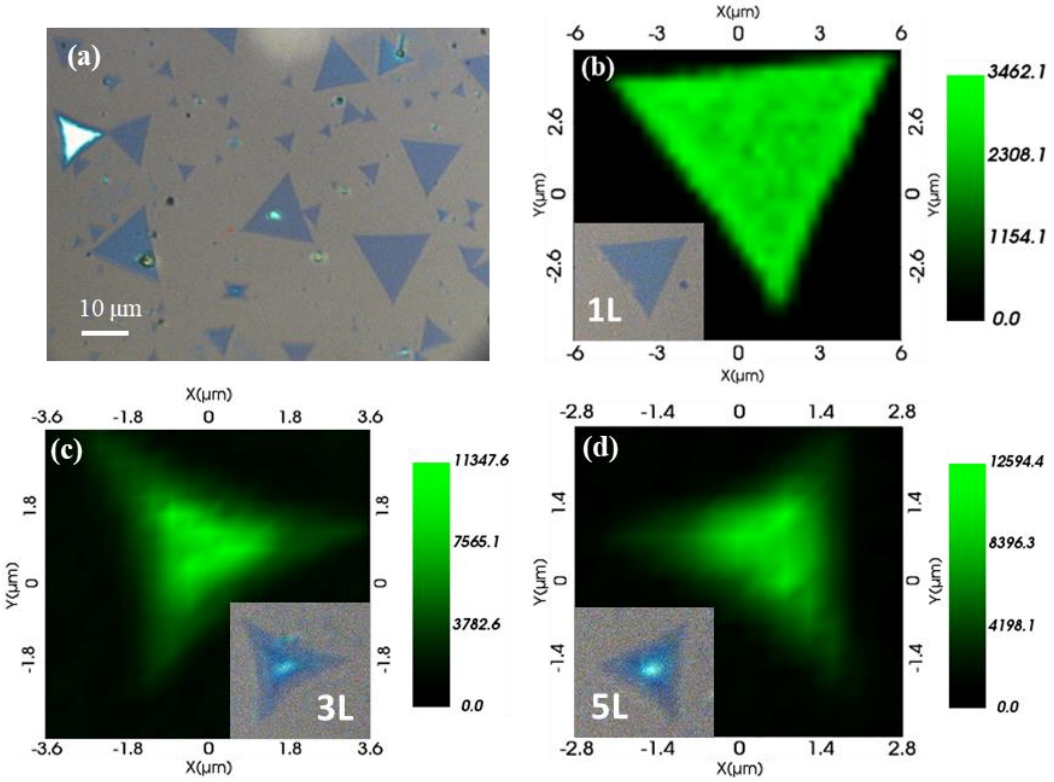

Figure 4.5 *(a) Optical image of CVD grown triangular MoS_2/SiO_2-Si. (b-d) Confocal Raman mapping of 1L, 3L and 5L triangular MoS_2. The corresponding optical image is shown in the inset.*

The SEM image of prepared MoS_2 film is shown in **Figure 2.8 (a)** of **chapter 2**, which exhibits nearly equilateral triangular shapes of varying sizes. To confirm the number of atomic layers and phase formed, different layered MoS_2 nanoflakes have been characterized using Raman spectroscopy. **Figure 2.13 (a)** of **chapter 2** shows the Raman spectra for 1L, 3L and 5L triangular MoS_2 using 532 nm excitation source. Out of the possible 9 phonon modes at Γ point (for 1L) as suggested above via group theory and DFPT, only four phonon modes are considered as Raman active: A_1' (x^2+y^2 and z^2), E′ (x^2-y^2 and xy) and E″ (x and yz) [154]. The E′ (32 cm^{-1}) and E″ (286 cm^{-1}) modes are usually not observed because of strong Rayleigh line and backscattering geometry, respectively. Thus, MoS_2 shows only two prominent Raman peaks under non-resonant condition (532 nm) that reflect its crystal structure: E' (~384 cm^{-1})

and A_1'(~409 cm^{-1}). Instead of using different notations for modes in odd and even L, simply E^1_{2g} and A_{1g} notations are used for the ease of comparison, as commonly used in literature. The E^1_{2g} and A_{1g} modes are shifted with increasing layers and their separation gives a clear estimation of number of layers. This difference is observed to be 18.7 ± 0.3 cm^{-1}, 22.2 ± 0.2 cm^{-1} and 24.3 ± 0.3 cm^{-1} corresponding to 1L, 3L and 5L, respectively [123]. Resonant scattering (excitation energy close to the optical transition) results in the appearance of many other vibrational modes in addition to the forbidden modes because of the resonance effect and broken symmetry. The 633 nm excitation laser (1.96 eV) resonates with the A exciton energy of MoS_2, showing in additional phonon modes at M-point that evolve with layer number, providing rich information about phonons in the entire BZ. **Figure 2.13 (c)** of **chapter 2** shows the resonant Raman spectra for 1L, 3L and 5L triangular MoS_2 with 633 nm excitation source. In 1L MoS_2, quantum confinement results in increased transition energy at K-point. This leads to weak coupling between excitonic transition at K-point with phonons and hence the phonon modes show negligible intensity in 1L MoS_2 [122].

4.2.3.2 Anisotropic Response

(A) Effect of Layer Number on Anisotropic Response

Figure 4.6 (a-d) shows the typical polarized Raman spectra of 1L MoS_2 nanoflake from θ = 0-90°, 100-180°, 190-270° and 280-360°, respectively, at the interval of 10° under non-resonant excitation. Under parallel configuration ($\hat{g}_i \parallel \hat{g}_s$), the intensity of A_{1g} phonon mode is greater than the intensity of E^1_{2g} phonon mode, while under perpendicular configuration ($\hat{g}_i \perp \hat{g}_s$), the intensity of A_{1g} phonon mode is significantly smaller (almost diminishes) than the intensity of E^1_{2g} phonon mode. To observe the effect of layer dependency, polarized Raman spectra for 3L **(Figure 4.7)** and 5L **(Figure 4.8)** triangular MoS_2 from θ = 0° to 360° have also been performed. **Figure 4.9 (a, b)** shows the comparative polar plots for E^1_{2g} and A_{1g} phonon intensities in 1L, 3L and 5L triangular MoS_2 as a function of θ, respectively. The isotropic

nature of the E^1_{2g} mode is observed in our experimental configuration, i.e. it remains constant with θ, while the Raman intensity of A_{1g} phonon mode displays a two-lobe shape of sinusoidal behavior that reaches a maximum at θ = 0° and 180° ($\hat{g}_i \parallel \hat{g}_s$) and diminishes at θ = 90° and 270° ($\hat{g}_i \perp \hat{g}_s$). Multiple data have been collected and incorporated in the polar plot as an error bar for standard deviation. This study suggests that anisotropic behavior (normalized polar plot) of both phonon modes (E^1_{2g} and A_{1g}) for MoS_2 remain unchanged with varying layer number. As the layer number increases, the electronic transition energy decreases and thus the coupling between electronic transitions and phonons becomes stronger on excitation with particular wavelength [155-157]. Thus, increasing layer number of MoS_2 only varies the intensity of phonon modes under a particular excitation wavelength and the anisotropic behavior of the phonon modes (either E^1_{2g} and A_{1g}) for MoS_2 remain unchanged with varying layer numbers.

In order to understand the anisotropic behavior of E^1_{2g} and A_{1g} phonon mode, the intensity of the Raman-active modes is given by the proportionality relation [158, 159]-

$$I(j) \propto |\hat{g}_s \cdot R(j) \cdot \hat{g}_i|^2 \tag{4.1}$$

Thus, a phonon mode can be detected only if the term $|\hat{g}_s \cdot R(j) \cdot \hat{g}_i|^2$ acquires a non-zero value. The E^1_{2g} phonon mode has two degenerate states: (E^1_{2g}, xy) and (E^1_{2g}, x^2-y^2), corresponding to one LO and one TO phonon branch, respectively. The incident excitation induces deformation in the phonon modes of the crystal and thus, the electron-phonon interaction occurs via deformation potential (DP). In **equation 4.1**, the DP Raman tensors for E^1_{2g} and A_{1g} phonon modes in odd number of layers (D_{3h}) are obtained from the character table (**Table 4.1**), that takes the following forms [160]-

$$R\,(E^1_{2g}, xy)^{DP} = \begin{pmatrix} 0 & d' & 0 \\ d' & 0 & 0 \\ 0 & 0 & 0 \end{pmatrix} \text{ and } R\,(E^1_{2g}, x^2\text{-}y^2)^{DP} = \begin{pmatrix} d & 0 & 0 \\ 0 & -d & 0 \\ 0 & 0 & 0 \end{pmatrix} \tag{4.2}$$

$$R\,(A_{1g}, x^2+y^2 \text{ and } z^2)^{DP} = \begin{pmatrix} a & 0 & 0 \\ 0 & a & 0 \\ 0 & 0 & b \end{pmatrix} \tag{4.3}$$

Here, a, b, d and d′ are major terms in the Raman tensor matrix and describes the physics of interaction between light and crystal symmetry. Other terms are negligible and taken as zero due to symmetry. The incoming light propagates along the x direction with polarization unit vectors given by: $\hat{g}_i = \begin{pmatrix} g_x \\ 0 \\ 0 \end{pmatrix} + e^{i\phi} \begin{pmatrix} 0 \\ g_y \\ 0 \end{pmatrix} = \begin{pmatrix} 1 \\ 0 \\ 0 \end{pmatrix}$

Since $g_x = 1$, $g_y = 0$ and $\phi = 0$ for horizontally polarized light, and after passing through the half-wave plate with rotation of α/2, it becomes $\hat{g}_i = \begin{pmatrix} \cos\alpha \\ \sin\alpha \\ 0 \end{pmatrix}$. Now, after fixing the direction of $\hat{g}_i$, we have rotated the analyzer from θ = 0° to 90°, at an interval of 10° and the scattered light goes along the xy plane in backscattering geometry with polarization unit vector: $\hat{g}_s$ = (cos (θ+α), sin (θ+α), 0), where θ is the angle between $\hat{g}_i$ and $\hat{g}_s$. As the E^1_{2g} phonon mode is doubly degenerate having two Raman tensors and so the total intensity of this mode is equal to the sum of Raman intensities involving each of the Raman tensors. Thus, we separately consider four different coordinates for our experimental setup and calculate the intensity of E^1_{2g} and A_{1g} phonon modes using **equation 4.1-4.3**.

(1) α/2 = 0º and θ = 0º to 90º

$\hat{g}_i = \begin{pmatrix} 1 \\ 0 \\ 0 \end{pmatrix}$ and $\hat{g}_s = (\cos\theta, \sin\theta, 0)$

$$I(E^1_{2g}) \propto \left| (\cos\theta, \sin\theta, 0). \begin{pmatrix} 0 & d' & 0 \\ d' & 0 & 0 \\ 0 & 0 & 0 \end{pmatrix}. \begin{pmatrix} 1 \\ 0 \\ 0 \end{pmatrix} \right|^2 + \left| (\cos\theta, \sin\theta, 0). \begin{pmatrix} d & 0 & 0 \\ 0 & -d & 0 \\ 0 & 0 & 0 \end{pmatrix}. \begin{pmatrix} 1 \\ 0 \\ 0 \end{pmatrix} \right|^2$$

$$\propto |d' \sin\theta|^2 + |d \cos\theta|^2$$

$$I(A_{1g}) \propto \left| (\cos\theta, \sin\theta, 0). \begin{pmatrix} a & 0 & 0 \\ 0 & a & 0 \\ 0 & 0 & b \end{pmatrix}. \begin{pmatrix} 1 \\ 0 \\ 0 \end{pmatrix} \right|^2 \propto |a \cos\theta|^2$$

(2) α/2 = 45º and θ = 0º to 90º

$\hat{g}_i = \begin{pmatrix} 0 \\ 1 \\ 0 \end{pmatrix}$ and $\hat{g}_s$ = (-sin θ, cos θ, 0)

$I(E^1_{2g}) \propto |-d' \sin\theta|^2 + |-d \cos\theta|^2$ and $I(A_{1g}) \propto |a \cos\theta|^2$

(3) $\alpha/2 = 90^o$ and $\theta = 0^o$ to 90^o

$$\hat{g}_i = \begin{pmatrix} \overline{1} \\ 0 \\ 0 \end{pmatrix} \quad \text{and} \quad \hat{g}_s = (-\cos\theta, -\sin\theta, 0)$$

$I(E^1_{2g}) \propto |d' \sin\theta|^2 + |d \cos\theta|^2$ and $I(A_{1g}) \propto |a \cos\theta|^2$

(4) $\alpha/2 = 135^o$ and $\theta = 0^o$ to 90^o

$$\hat{g}_i = \begin{pmatrix} 0 \\ \overline{1} \\ 0 \end{pmatrix} \quad \text{and} \quad \hat{g}_s = (\sin\theta, -\cos\theta, 0)$$

$$I(E^1_{2g}) \propto |-d' \sin\theta|^2 + |-d \cos\theta|^2 \tag{4.4}$$

$$I(A_{1g}) \propto |a \cos\theta|^2 \tag{4.5}$$

When fitted the E^1_{2g} phonon modes, we got $d' \cong d$, indicating the constant behavior of E^1_{2g} phonon mode, while A_{1g} phonon mode shows the θ dependent anisotropic response i.e., maximum at $\theta = 0°$ and 180° (when $\hat{g}_i$ and $\hat{g}_s$ are parallel) and decreases monotonically to 0 when $\hat{g}_i$ and $\hat{g}_s$ are perpendicular to each other. Solid line in **Figure 4.9 (a, b)** represents the fitted curve of E^1_{2g} and A_{1g} phonon modes using these equations in different layered triangular MoS_2 and thus, the fitted curves are in good agreement with Raman tensor analysis. The anisotropy of E^1_{2g} and A_{1g} phonon modes for other layer numbers (3L and 5L) shows the consistent results, irrespective of the layer number with only minor differences in the lobe size i.e., as the thickness increases the lobe size increases. Thus, the polarization behavior of E^1_{2g} and A_{1g} phonon modes agrees well with the polarization selection rule under non-resonant excitation.

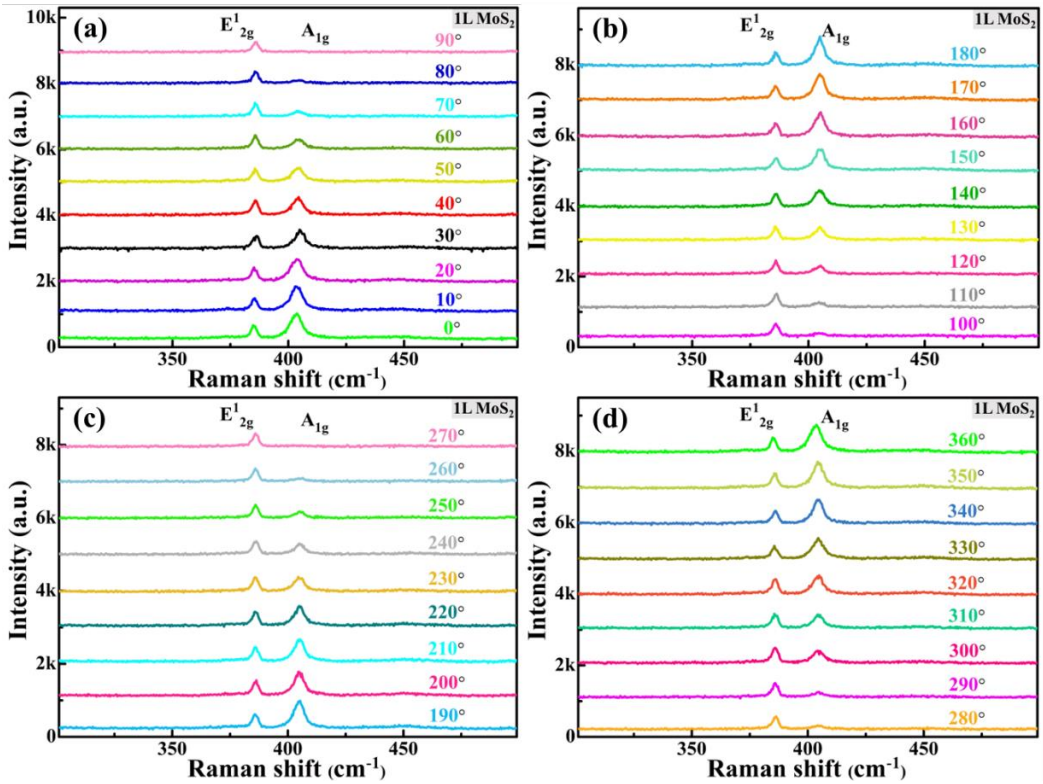

Figure 4.6 *Polarized Raman spectra of 1L CVD grown triangular MoS_2 nanostructure from (a) θ = 0° to 90°, (b) 100° to 180°, (c) 190° to 270° and (d) 280° to 360°, at an interval of 10°, obtained using 532 nm excitation.*

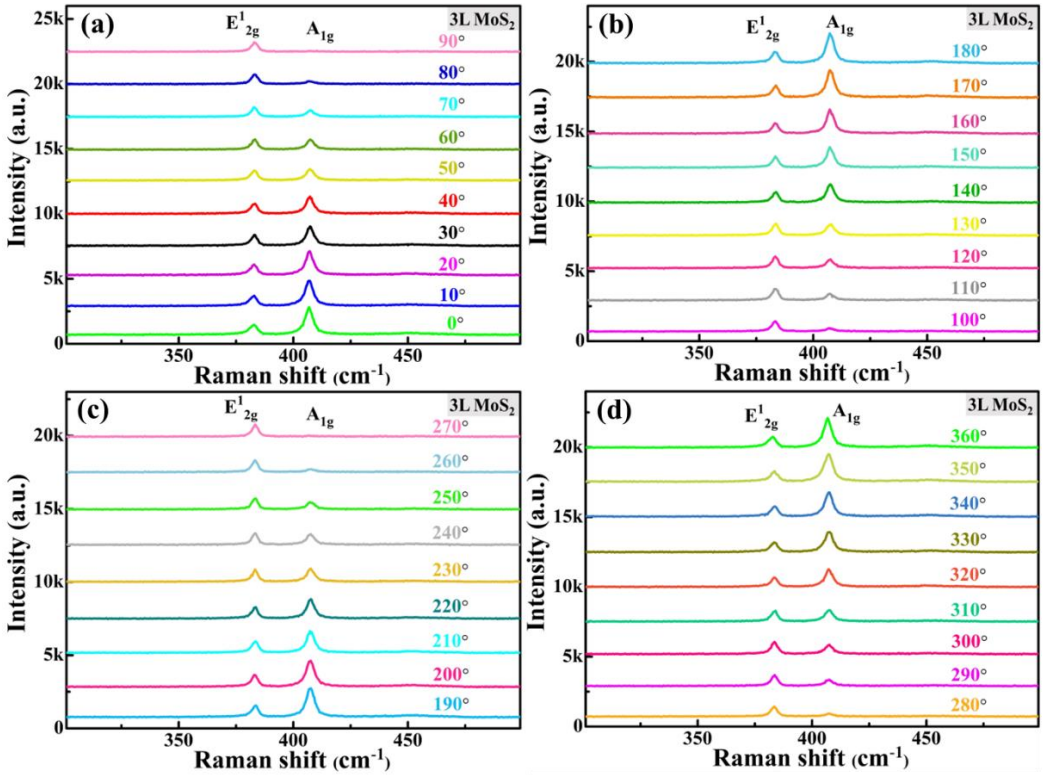

Figure 4.7 *Polarized Raman spectra of 3L CVD grown triangular MoS_2 nanostructure from (a) θ = 0° to 90°, (b) 100° to 180°, (c) 190° to 270° and (d) 280° to 360°, at an interval of 10°, obtained using 532 nm excitation.*

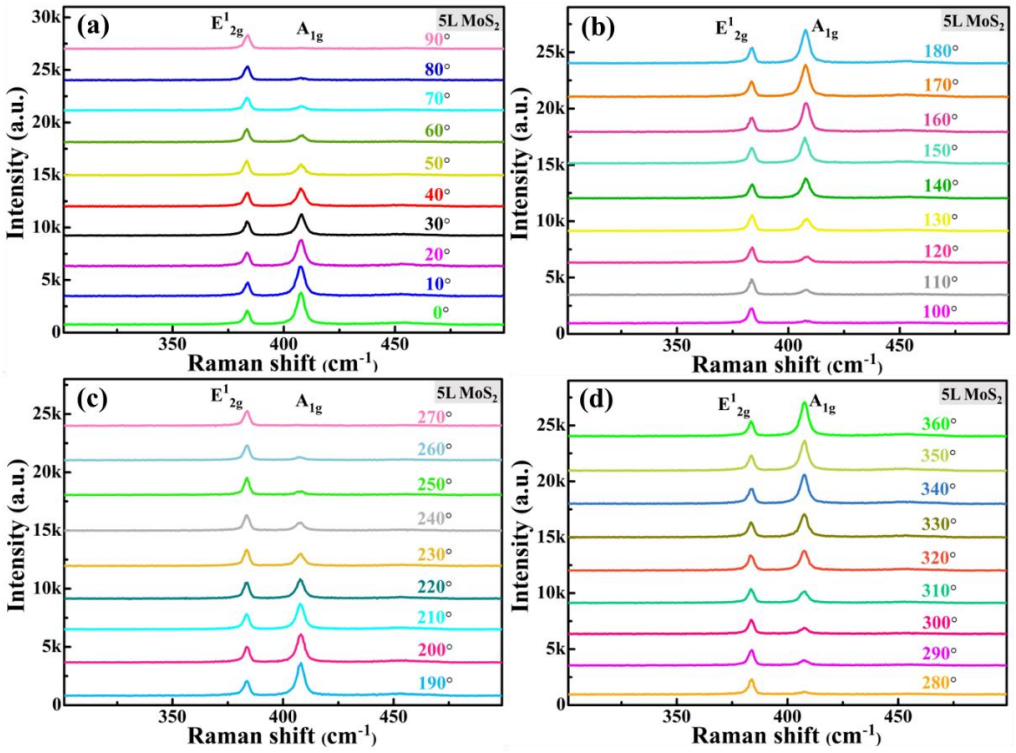

Figure 4.8 *Polarized Raman spectra of 5L CVD grown triangular MoS_2 nanostructure from (a) θ = 0° to 90°, (b) 100° to 180°, (c) 190° to 270° and (d) 280° to 360°, at an interval of 10°, obtained using 532 nm excitation.*

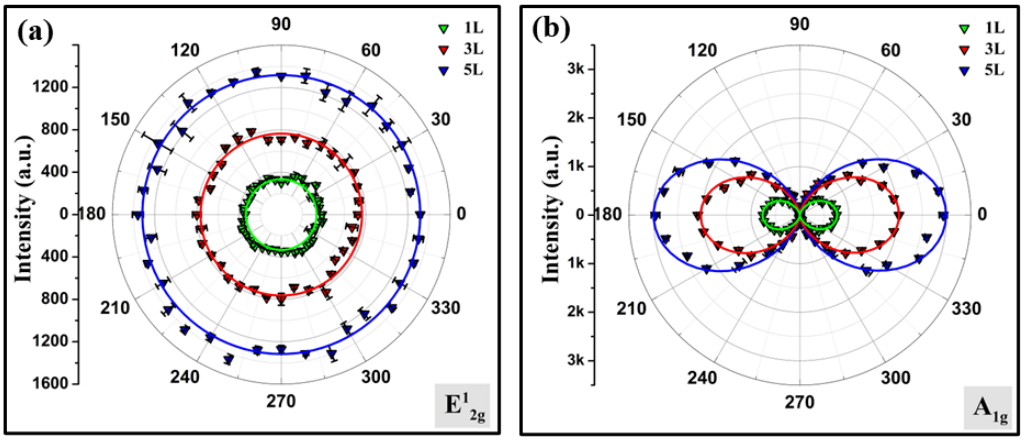

Figure 4.9 *Polar plots of layer dependent (1L, 3L and 5L) triangular MoS_2 for (c) E^1_{2g} and (d) A_{1g} phonon mode.*

(B) Effect of Excitation wavelength on Anisotropic Response

In order to examine the effect of electron-photon coupling on the anisotropic behavior of MoS_2, we have performed ARPRS study of prepared MoS_2 with resonant (633 nm) excitation source as well. Since 1L MoS_2 does not show significant Raman peak with 633 nm excitation (as shown in **Figure 2.13 (c)** of **chapter 2**), hence we have carried out the ARPRS

study for 3L and 5L triangular MoS_2. **Figure 4.10 (a-d)** shows the complete polarization study for 3L MoS_2 from θ = 0° to 360°, at the interval of 10° with resonant excitation. The polarized Raman spectra for 5L MoS_2 with resonant excitation is shown in **Figure 4.11**.

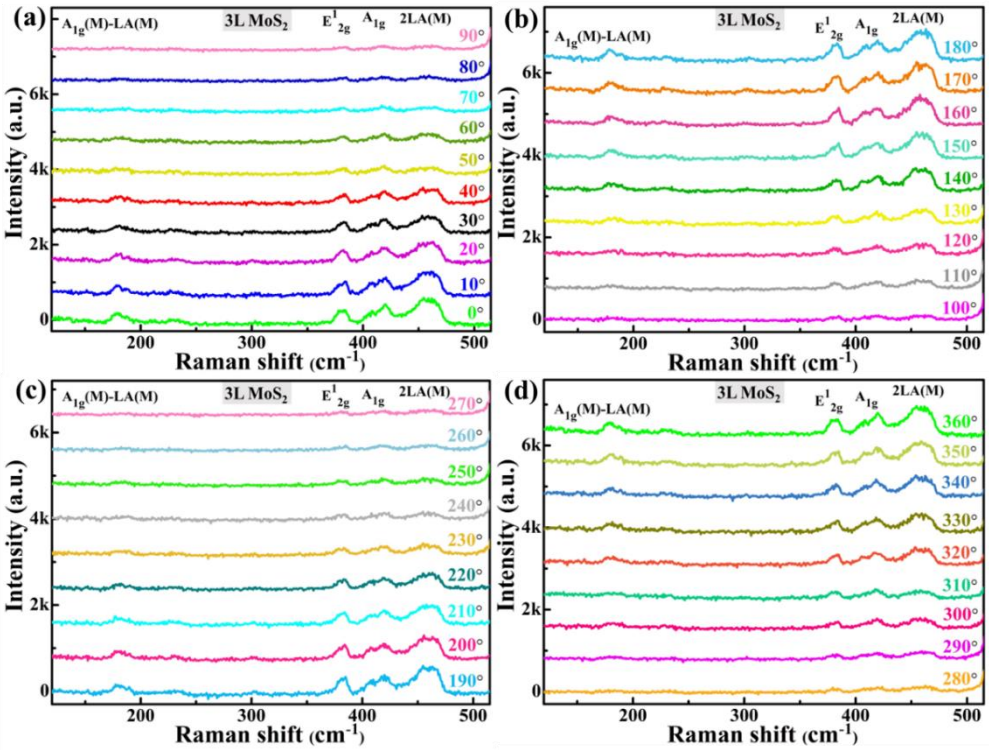

Figure 4.10 *Polarized Raman spectra of 3L CVD grown triangular MoS_2 nanostructure from (a) θ = 0° to 90°, (b) 100° to 180°, (c) 190° to 270° and (d) 280° to 360°, at an interval of 10°, obtained using 633 nm excitation.*

The polarization behavior of E^1_{2g} Raman modes with 633 nm excitation is in stark contrast to the response with 532 nm excitation. The E^1_{2g} phonon mode is no more invariant with rotation but exhibits anisotropic nature with intensity at θ = 0° and 180° ($\hat{g}_i \parallel \hat{g}_s$) greater than intensity at θ = 90° and 270° ($\hat{g}_i \parallel \hat{g}_s$) with resonant excitation, while the polarization behavior of A_{1g} phonon mode shows similar anisotropic response as observed for non-resonant excitation, as shown in **Figure 4.12 (a, b)**. In addition to these two modes in the Raman spectra with 633 nm excitation, two intense bands: A_{1g}(M) – LA (M) and 2LA(M) are also observed to exhibit the similar anisotropic behavior like A_{1g} phonon modes, as observed in polar plots of **Figure 4.12 (c, d)**.

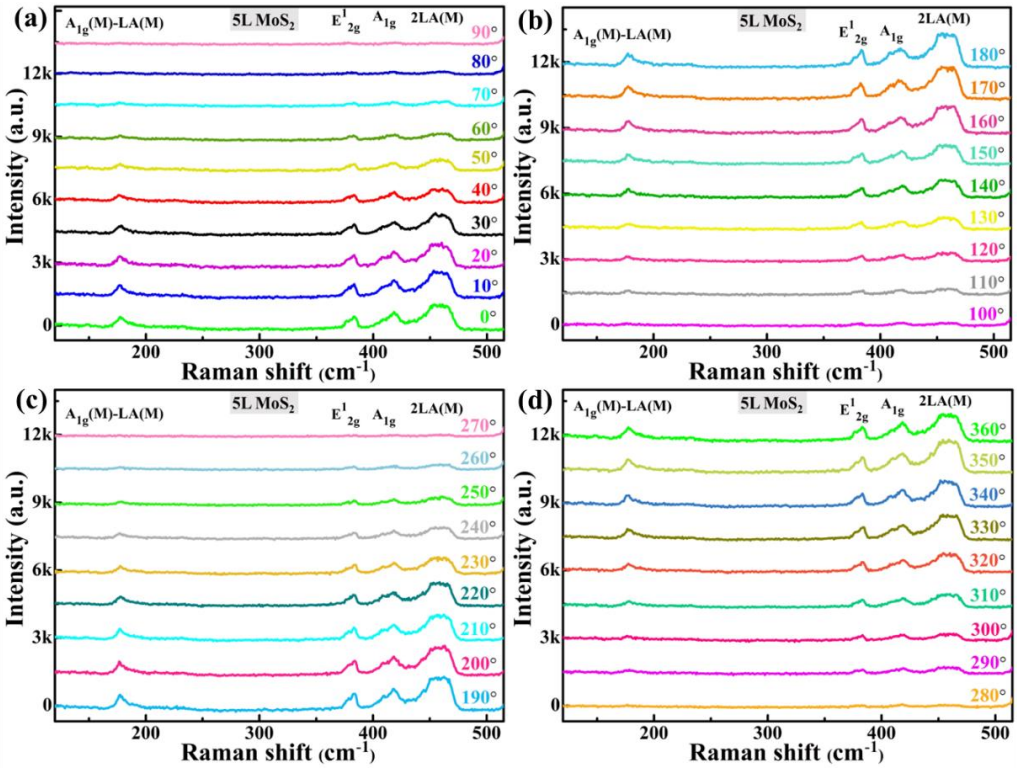

Figure 4.11 *Polarized Raman spectra of 5L CVD grown triangular MoS_2 nanostructure from (a) θ = 0° to 90°, (b) 100° to 180°, (c) 190° to 270° and (d) 280° to 360°, at an interval of 10°, obtained using 633 nm excitation.*

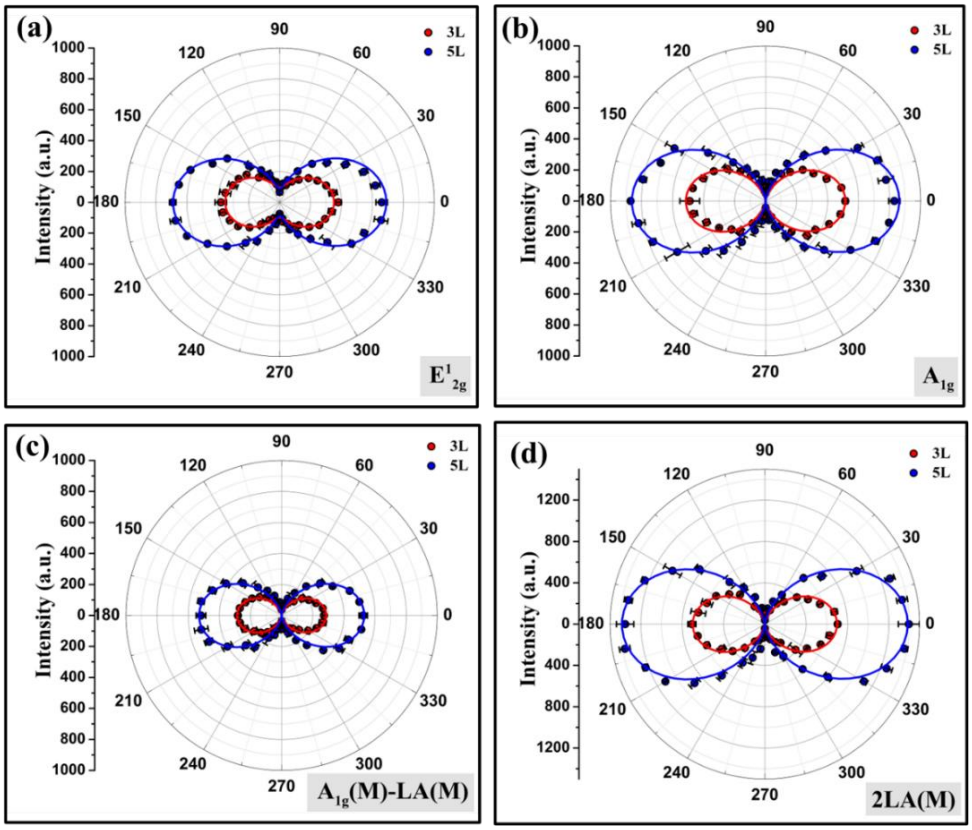

Figure 4.12 *Polar plots of layer dependent (3L and 5L) MoS_2 for (a) E^1_{2g}, (b) A_{1g}, (c) A_{1g}(M) – LA (M) and (d) 2LA(M) phonon modes.*

The different anisotropic behavior of E^1_{2g} depends upon excitation source due to possible electron-phonon-photon coupling. Under resonant condition, the LO phonon mode involves the displacement of the oppositely charged atoms that induces a macroscopic electric field [161, 162]. This electric field couples with electrons or excitons similar to piezoelectric electric field of acoustic phonons, known as Fröhlich interaction (FI) [163, 164]. The Raman tensor for scattering owing to Fröhlich interaction is given by [62]-

$$R\,(E^1_{2g}, xy)^{FI} = \begin{pmatrix} c & 0 & 0 \\ 0 & c & 0 \\ 0 & 0 & c \end{pmatrix} \tag{4.6}$$

Thus, the intensity for E^1_{2g} phonon mode is given by:

$$I(E^1_{2g}) \propto |\hat{g}_s \cdot [R(E^1_{2g}, xy)^{DP} + R(E^1_{2g}, xy)^{FI}] \cdot \hat{g}_i|^2 + |\hat{g}_s \cdot R(E^1_{2g}, x^2\text{-}y^2)^{DP} \cdot \hat{g}_i|^2$$

$$\propto |c \cos\theta + d' \sin\theta|^2 + |d \cos\theta|^2 \tag{4.7}$$

The overall fitting of the anisotropic response of E^1_{2g} phonon modes with 633 nm excitation is found good with **equation 4.7**. While the A_{1g} phonon mode maintains the similar anisotropic behavior under resonant and non-resonant excitation and thus, we have fitted the polarization behavior of A_{1g} phonon mode using the same equation as for non-resonant excitation case. For A_{1g}(M) – LA (M) and 2LA(M) modes, same fitting equations are used because of similar anisotropic behavior. Thus, the theory incorporating the Frohlich interaction completely explains the polarization behavior of triangular MoS_2 film under resonant excitation.

4.2.4 ARPRS Study of Horizontally Grown MoS_2 over SiO_2-Si Substrate (H-MoS_2/SiO_2-Si)

In this section, similar polarisation study we have performed on H-MoS_2/SiO_2-Si using ARPRS technique under two different excitations (non-resonant and resonant) to reveal the electron-phonon-photon interaction in prepared MoS_2 film. The SEM image of prepared H-MoS_2/SiO_2-Si film (**Figure 2.8 (b)** of **chapter 2)** illustrates a uniform and continuous thin layer formation. The observable separation (~24 cm^{-1}) between E^1_{2g} and A_{1g} peaks in Raman

spectrum (**Figure 2.13 (b)** of **chapter 2**) and height profile of AFM image (**Figure 2.10 (d)** of **chapter 2**) of H-MoS_2/SiO_2-Si suggests the growth of five-layers in horizontal oriented MoS_2 thin film [92, 93]. **Figure 4.13 (a-d)** shows the complete polarized Raman spectra from 0º to 360º, at an interval of 10º. **Figure 4.13 (e)** shows the corresponding polar plots for both the phonon modes (E^1_{2g} and A_{1g}) of MoS_2, observed under non-resonant excitation (532 nm).

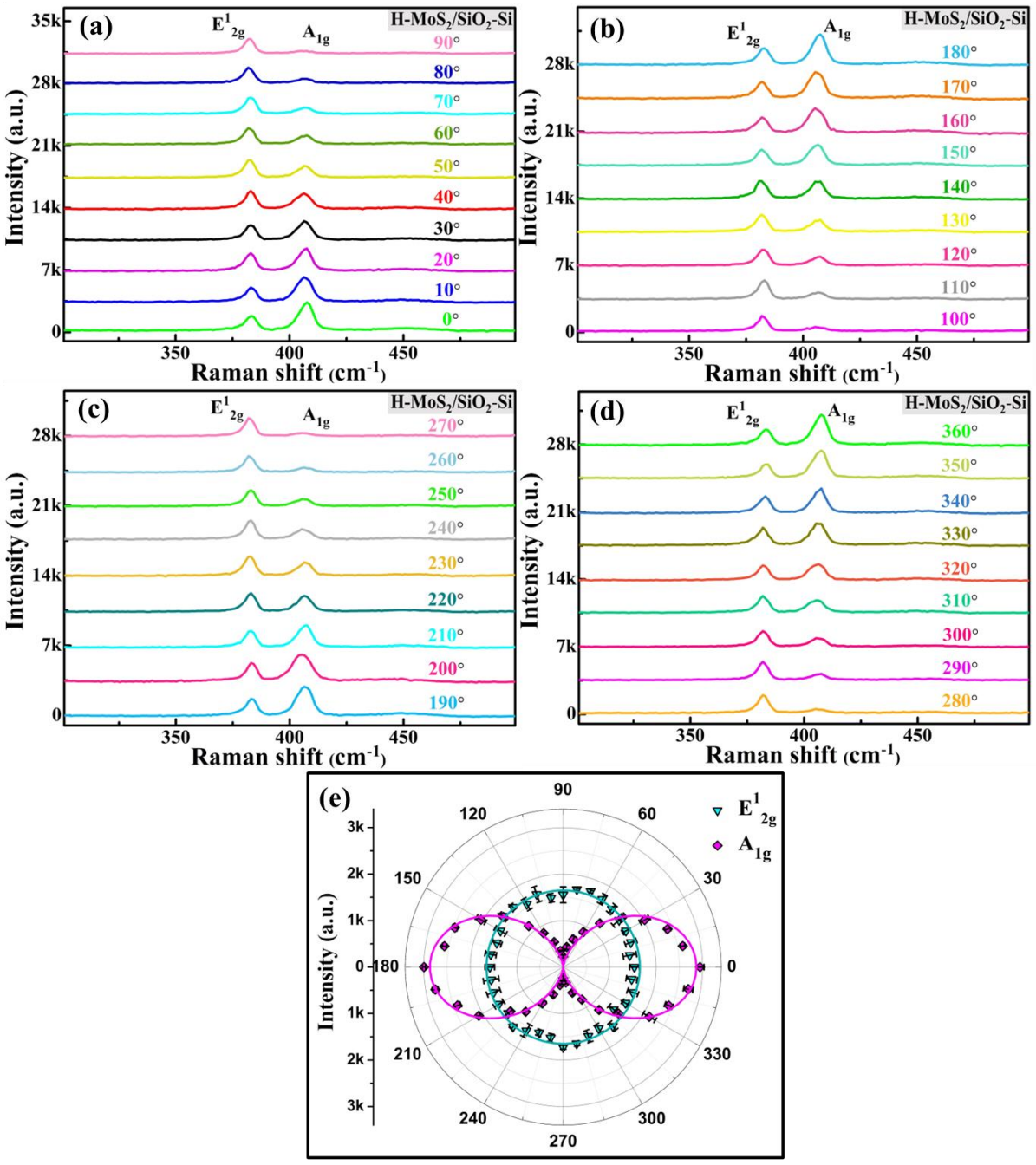

Figure 4.13 *Polarized Raman spectra of H-MoS_2/SiO_2-Si from (a) θ = 0° to 90°, (b) 100° to 180°, (c) 190° to 270° and (d) 280° to 360°, at an interval of 10°, obtained using 532 nm excitation. (e) Polar plots of H-MoS_2/SiO_2-Si for E^1_{2g} and A_{1g} phonon mode.*

Similar behavior has been observed for both the phonon modes as for triangular MoS_2, i.e., E^1_{2g} phonon mode displays isotropic behavior with no θ dependence, while the A_{1g} phonon mode exhibits strong anisotropic response with maximum intensity for parallel (θ = 0º) and almost negligible intensity for perpendicular (θ = 90º) configuration, displaying a two-lobe sinusoidal pattern. Thus, we fit the polar plots of E^1_{2g} and A_{1g} phonon modes using same **equation 4**: $I(E^1_{2g}) \propto |d' \sin\theta|^2 + |d \cos\theta|^2$ and $I(A_{1g}) \propto |a \cdot \cos\theta|^2$, finding good agreement for non-resonant excitation.

To explore the impact of electron-phonon-photon coupling on the anisotropic response of these modes, we have conducted measurements using resonant excitation (633 nm) as well. **Figure 4.14 (a-d)** displays complete polarized Raman spectra from 0º to 360º at 10º intervals under 633 nm excitation, along with corresponding polar plots for E^1_{2g} and A_{1g} phonon modes in **Figure 4.14 (e)**. Similar behavior like triangular MoS_2 is observed on switching excitation from non-resonant (532 nm) to resonant (633 nm), i.e., A_{1g} mode maintains anisotropic response while the E^1_{2g} mode shifts from isotropic to anisotropic. Studying other intense modes with 633 nm excitation: A_{1g}(M) – LA(M) and 2LA(M), reveals a similar two-lobe anisotropic response. Thus, by incorporating FI, the polar plot for E^1_{2g} phonon mode is fitted using the same **equation 4.7** as for E^1_{2g} phonon mode in triangular MoS_2 under resonant excitation. This fitting of the E^1_{2g} phonon mode under resonant excitation aligns well with this modified equation, while the response of the A_{1g} mode remains similar to non-resonant excitation and thus A_{1g}, A_{1g}(M) – LA(M) and 2LA(M) phonon modes are fitted using the same **equation 4.5**.

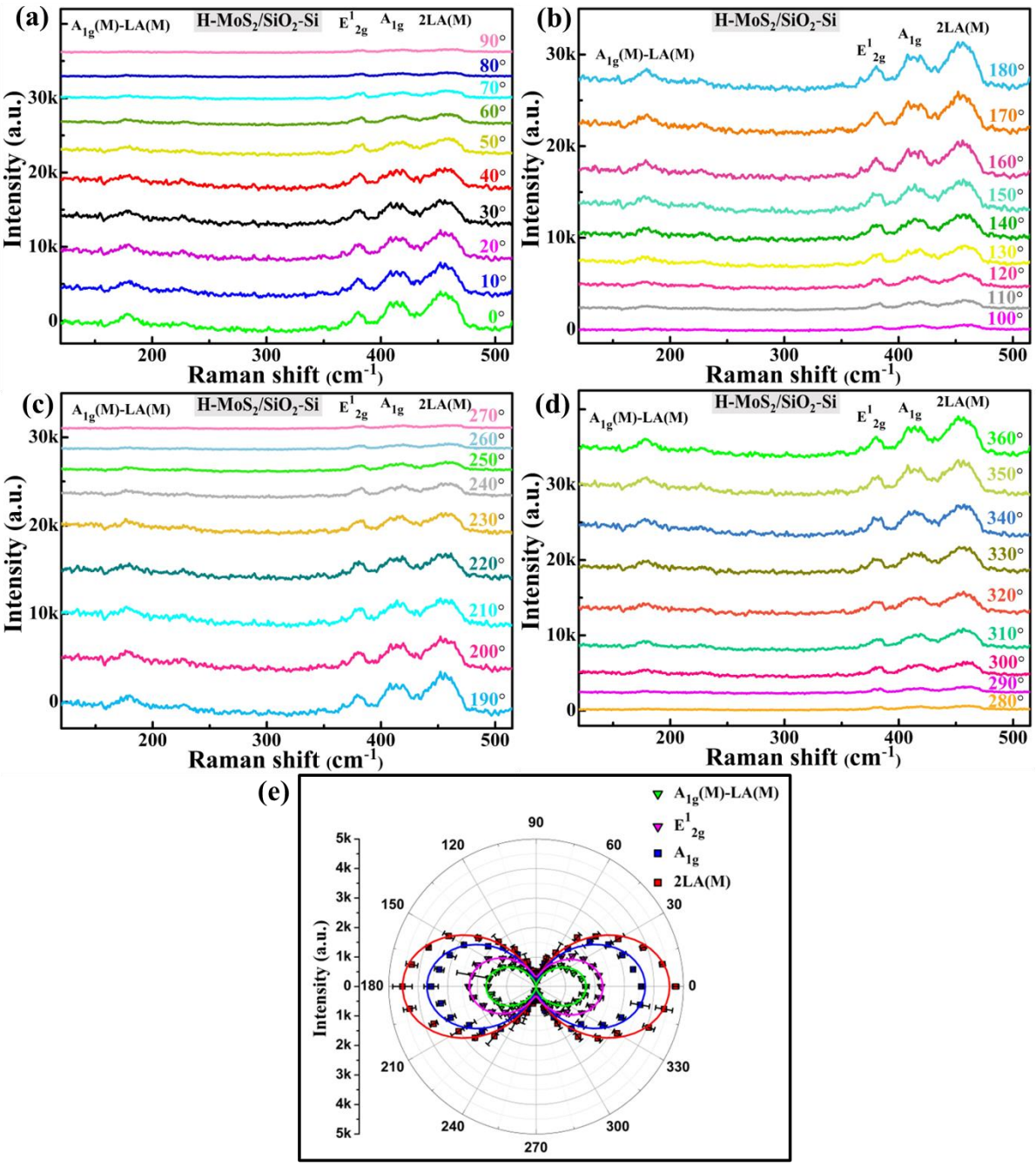

Figure 4.14 *Polarized Raman spectra of H-MoS_2/SiO_2-Si from (a) θ = 0° to 90°, (b) 100° to 180°, (c) 190° to 270° and (d) 280° to 360°, at an interval of 10°, obtained using 633 nm excitation. (e) Polar plots of H-MoS_2/SiO_2-Si for E^1_{2g}, A_{1g}, A_{1g}(M) – LA (M) and 2LA(M) phonon mode.*

4.2.5 ARPRS Study of Vertically Grown MoS_2 over SiO_2-Si Substrate (V-MoS_2/SiO_2-Si)

All the above studies in this chapter have been performed on horizontally oriented nanostructures of MoS_2 (triangular MoS_2 and H-MoS_2/SiO_2-Si). To illustrate the effect of orientation of MoS_2 nanostructure with substrate on anisotropic response, the ARPRS study of

vertically oriented MoS_2 nanostructures grown over the same substrate (V-MoS_2/SiO_2-Si) have been performed under non-resonant and resonant excitations in this section. The SEM image of the prepared V-MoS_2/SiO_2-Si **(Figure 4.15 (a))** depicts the formation of vertically oriented 3D network of MoS_2 nanoflakes. **Figure 4.15 (b-e)** shows the complete polarized Raman spectra from 0 to 360º, at an interval of 10º. Under parallel configuration, the intensity of A_{1g} phonon mode exceeds the intensity of E^1_{2g} phonon mode, while under perpendicular configuration, the intensity of A_{1g} mode decreases significantly compared to E^1_{2g} mode. The separation of ~24.6 cm^{-1} between E^1_{2g} and A_{1g} phonon mode suggesting the growth of nearly five to six layers in V-MoS_2/SiO_2-Si. The polar plots (**Figure 4.15 (f)**) depict the intensity of E^1_{2g} and A_{1g} mode in V-MoS_2/SiO_2-Si as a function of θ. It is observed that the anisotropic response of E^1_{2g} phonon modes in V-MoS_2/SiO_2-Si under 532 nm excitation shows deviation from isotropic behavior (circular polar plot) of horizontally oriented films, and exhibit anisotropic response, with intensity at θ = 0° and 180° greater than the intensity at θ = 90° and 270°. Hence, this response has been fitted using the combined function, i.e., $a^2\cos^2\theta + d^2$. Similarly, the anisotropic response of A_{1g} phonon modes of V-MoS_2/SiO_2-Si also follows the same function. The different anisotropic response of V-MoS_2/SiO_2-Si compared to horizontally oriented film of MoS_2 is observed due to the symmetry breaking at the exposed edges of the vertical nanosheets, which are oriented at different angles with the substrate [165]. Similar anisotropic Raman response has also been reported for nanoribbon of different ribbon widths and for MoS_2/nanowire heterostructure due to symmetry breaking [39, 166, 167]. To examine the influence of electron-phonon-photon coupling on the anisotropic response of these modes in V-MoS_2/SiO_2-Si, we performed measurements using resonance excitation (633 nm) as well. **Figure 4.16 (a-d)** shows the complete polarized Raman spectra from 0 to 360º, at 10º intervals under 633 nm excitation. The corresponding polar plots for intense modes: A_{1g}(M) – LA(M),

E^1_{2g}, A_{1g} and 2LA(M) are shown in **Figure 4.16 (e)**. All the modes follow the same combined function, i.e., $a^2\cos^2\theta + d^2$, due to symmetry breaking in vertically oriented nanosheets.

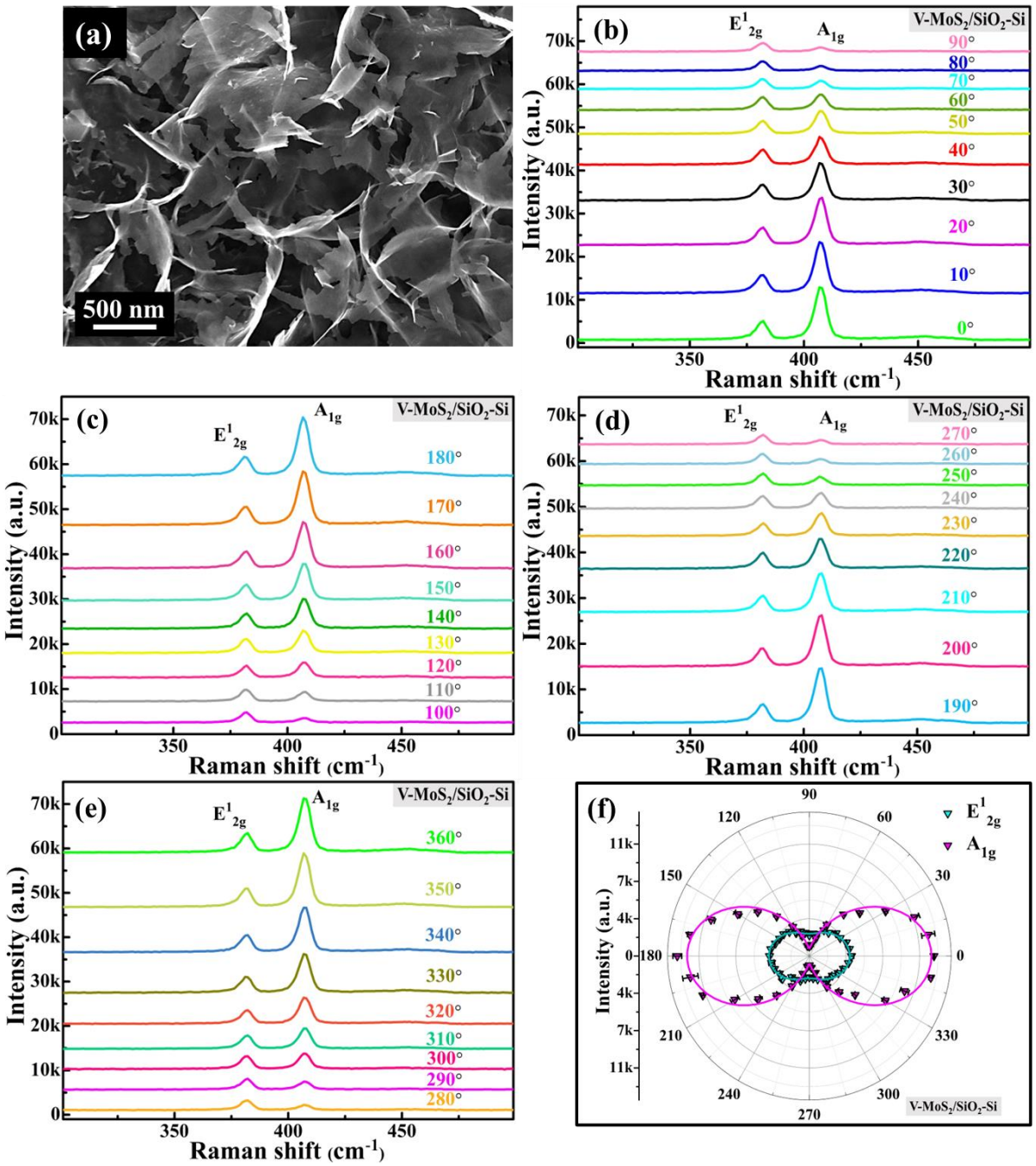

Figure 4.15 *(a) SEM image of V-MoS_2/SiO_2-Si. Polarized Raman spectra of V-MoS_2/SiO_2-Si from (b) 0° to 90°, (c) 100° to 180°, (d) 190° to 270° and (e) 280° to 360°, at an interval of 10°, obtained using 532 nm excitation (f) Polar plots of V-MoS_2/SiO_2-Si for E^1_{2g} and A_{1g} phonon mode with 532 nm excitation.*

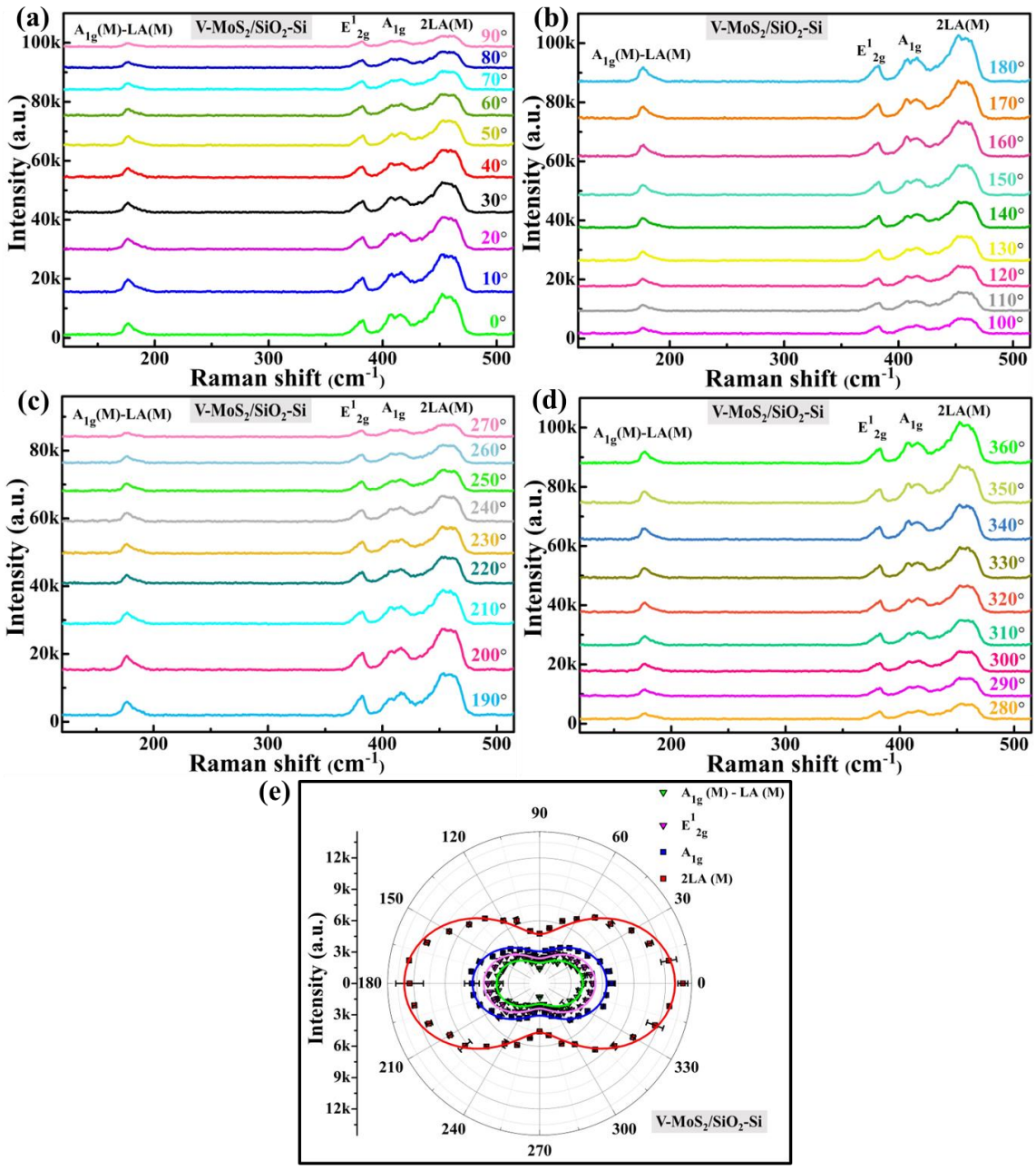

Figure 4.16 *Polarized Raman spectra of V-MoS_2/SiO_2-Si from (a) 0° to 90°, (b) 100° to 180°, (c) 190° to 270° and (d) 280° to 360°, at an interval of 10°, obtained using 633 nm excitation. (e) Polar plots of V-MoS_2/SiO_2-Si for E^1_{2g}, A_{1g}, A_{1g}(M) – LA (M) and 2LA(M) phonon mode.*

4.2.6 ARPRS Study of Horizontally Grown MoS_2 over FTO Coated Glass Substrate (H-MoS_2/FTO)

The previous sections deal with the optical anisotropic response of MoS_2 (horizontally/vertically oriented) grown over SiO_2-Si substrate. This section delves into the exploration of the optical anisotropic response of MoS_2 grown over a conducting substrate, i.e.,

FTO, aimed at elucidating the influence of substrate. **Figure 2.8 (d)** of **chapter 2** shows the SEM image of the prepared H-MoS_2/FTO, indicating the growth of continuous thin film of MoS_2. **Figure 2.13 (b)** of **chapter 2** shows the Raman spectrum of the prepared MoS_2 film with observed two prominent modes: E^1_{2g} mode at ~382 cm^{-1} (in-plane vibration of Mo and S atoms) and A_{1g} mode at ~407 cm^{-1} (out-of-plane vibration of S atoms). The separation of 25 cm^{-1} between these two prominent peaks suggests the growth of more than six layers, as suggested in literature [19, 168]. **Figure 4.17 (a-d)** shows the complete polarized Raman spectra from 0º to 360º, at an interval of 10º and corresponding polar plot for both the phonon modes (E^1_{2g} and A_{1g}) of MoS_2 under non-resonant excitation (532 nm) are given in **Figure 4.17 (e)**. The E^1_{2g} phonon mode is observed to show no θ dependence, i.e., exhibiting isotropic behavior, while the A_{1g} phonon mode seems to exhibit strong anisotropic response, showing two-lobe sinusoidal behavior with maximum intensity for parallel configuration and almost negligible intensity for perpendicular configuration. In order to understand the effect of electron-phonon-photon coupling on the anisotropic response of Raman active phonon modes, we carry out the measurement under resonant excitation (633 nm) as well. **Figure 4.18 (a-d)** shows the polarized Raman spectra from 0-360º, at an interval of 10º and corresponding polar plot for E^1_{2g} and A_{1g} phonon modes under 633 nm excitation are given in **Figure 4.18 (e)**. As observed from the spectra, the intensity of both the phonon modes (E^1_{2g} and A_{1g}) decreases with increasing polarization angle from θ = 0 to 90º, and again is observed to increase with increasing polarization angle, exhibiting two-lobe sinusoidal behavior. Thus, it is observed that on changing the excitation from non-resonant (532 nm) to resonant (633 nm), A_{1g} phonon mode maintains its anisotropic response while E^1_{2g} phonon mode changes its response from isotropic to anisotropic. Also, we have studied the anisotropic response of two other intense modes, observed with 633 nm excitation: A_{1g}(M) – LA(M) and 2LA(M), exhibiting similar two-lobe type of anisotropic response.

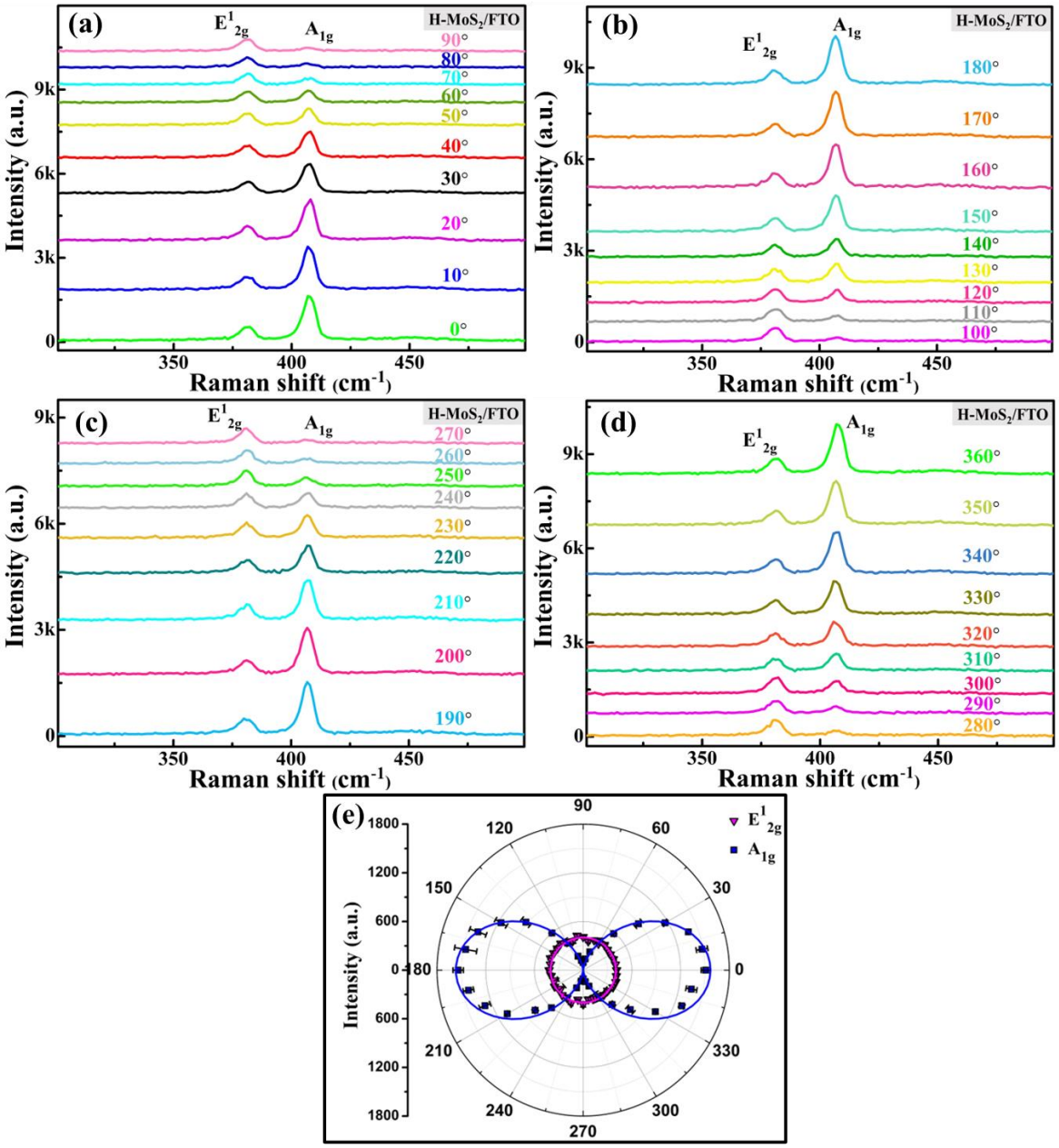

Figure 4.17 *Polarized Raman spectra of H-MoS_2/FTO from (a) θ = 0° to 90°, (b) 100° to 180°, (c) 190° to 270° and (d) 280° to 360°, at an interval of 10°, obtained using 532 nm excitation. (e) Polar plots of H-MoS_2/FTO for E^1_{2g} and A_{1g} phonon mode.*

Thus, we observe stark contrast in E^1_{2g} phonon mode under non-resonant and resonant excitation. To explain this anisotropic response, we consider similar approach, according to which: $I(E^1_{2g}) \propto |d' \sin\theta|^2 + |d \cos\theta|^2$ and $I(A_{1g}) \propto |a \cdot \cos\theta|^2$. Thus, we have fitted the polar plot of E^1_{2g} and A_{1g} phonon modes using these equations and result is in good agreement for non-resonant excitation. However, under resonant condition, Fröhlich interaction (FI) comes

into account and the fitting of E^1_{2g} phonon mode using equation $|c \cos \theta + d' \sin \theta|^2 + |d \cos \theta|^2$ in case of resonant excitation is found good. While the response of A_{1g} mode is similar as in case of non-resonant and thus A_{1g}, A_{1g}(M) – LA(M) and 2LA(M) phonon modes are fitted using the same equation, i.e., $|a \cdot \cos \theta|^2$. Thus, the anisotropic response is independent of the substrate over which MoS_2 is grown.

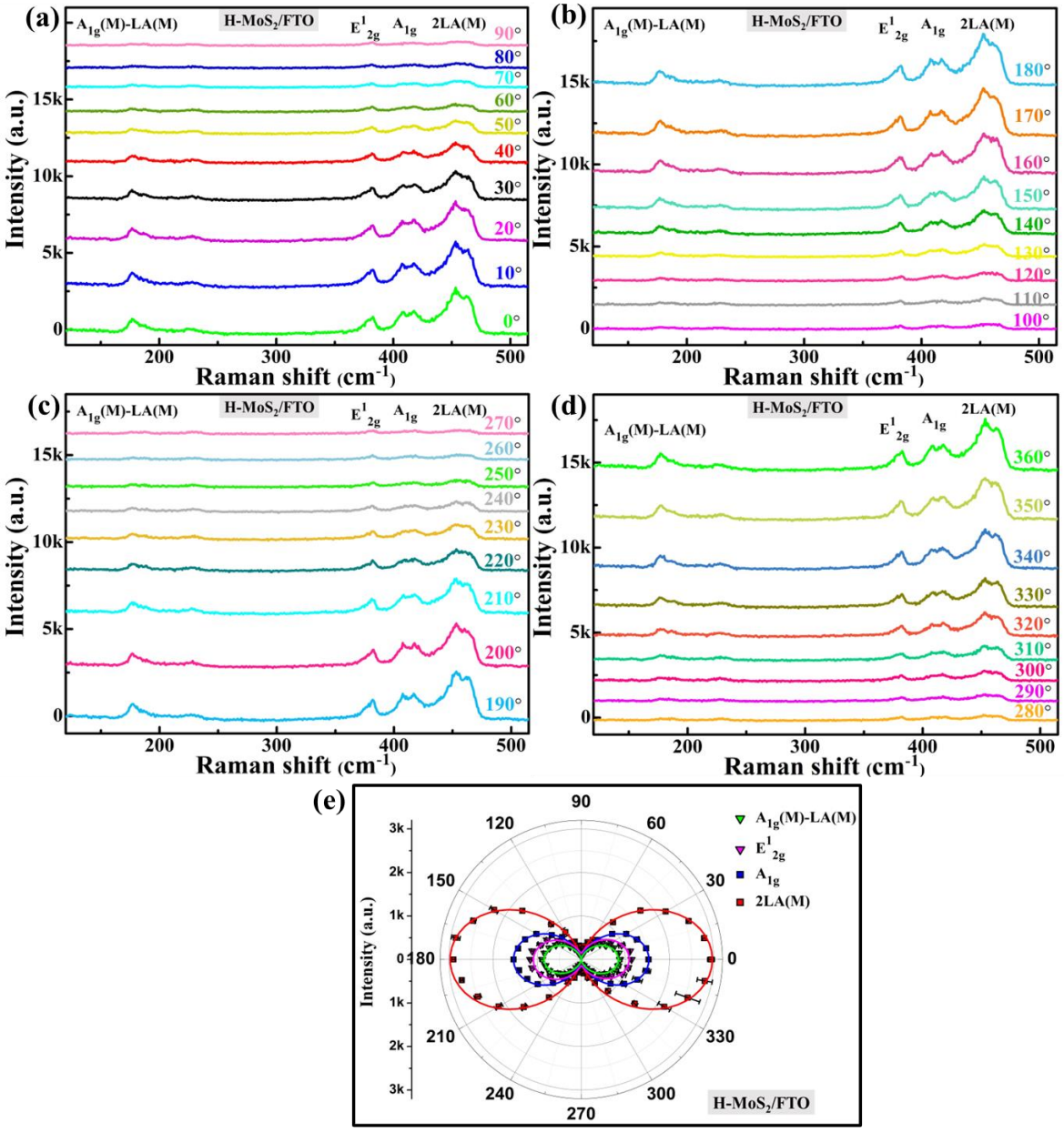

Figure 4.18 *Polarized Raman spectra of H-MoS_2/FTO from (a) θ = 0° to 90°, (b) 100° to 180°, (c) 190° to 270° and (d) 280° to 360°, at an interval of 10°, obtained using 633 nm excitation. (e) Polar plots of H-MoS_2/FTO for E^1_{2g}, A_{1g}, A_{1g}(M) – LA (M) and 2LA(M) phonon mode.*

4.3 Conclusion

In summary, we have theoretically calculated the phonon dispersion curve and phonon DOS for different layered (1 to 6L) MoS_2 nanostructures. Further, the polarization dependent anisotropic responses of phonon modes have been systematically studied using ARPRS study on CVD grown triangular MoS_2 as a function of layer number (1L, 3L and 5L) and incident excitation wavelength (532 and 633 nm). The results of ARPRS study are in agreement with the theory that includes the deformation potential. Under resonance condition, the variation in the polarization response of E^1_{2g} phonon mode is discussed by additionally incorporating Fröhlich electron-phonon interaction. Further we studied the anisotropic response of H-MoS_2/SiO_2-Si and V-MoS_2/SiO_2-Si under non-resonant and resonant excitation, to scrutinize the orientation effect. We also studied the anisotropic response of MoS_2 grown over conducting substrate (H-MoS_2/FTO), thereby elucidating no effect of the substrate over which MoS_2 is grown. One can enhance or suppress the absorption of light in specific directions by controlling the polarization of incident light, enabling the design of polarized photodetectors. It can be utilized to design optical modulators and switches that control the intensity or polarization of light. Thus, our study might be useful in the fabrication of polarization sensitive electronics and optoelectronic devices and to understand the responses of other TMDs as well.